

1 A strontium isoscape of Italy for provenance studies

2 Federico Lugli^{1,2*}, Anna Cipriani^{2,3*}, Luigi Bruno², Francesco Ronchetti², Claudio Cavazzuti^{4,5}, Stefano Benazzi^{1,6}

- 3 1. Department of Cultural Heritage, University of Bologna, Via degli Ariani 1, 48121 Ravenna, Italy.
- 4 2. Department of Chemical and Geological Sciences, University of Modena and Reggio Emilia, 41125 Modena, Italy.
- 5 3. Lamont-Doherty Earth Observatory, Columbia University, Palisades, New York 10964, USA.
- 6 4. Dipartimento di Storia Culture Civiltà, University of Bologna, 40124 Bologna, Italia.
- 7 5. Department of Archaeology, Durham University, Durham, United Kingdom.
- 8 6. Max Planck Institute for Evolutionary Anthropology, Department of Human Evolution, 04103 Leipzig, Germany.

9 *corresponding authors: federico.lugli6@unibo.it; anna.cipriani@unimore.it

10 Abstract

11 We present a novel database of environmental and geological $^{87}\text{Sr}/^{86}\text{Sr}$ values ($n = 1920$) from Italy, using literature
12 data and newly analysed samples, for provenance purposes. We collected both bioavailable and non-bioavailable
13 (i.e. rocks and bulk soils) data to attain a broader view of the Sr isotope variability of the Italian peninsula. These
14 data were used to build isotope variability maps, namely isoscapes, through Kriging interpolations. We employed
15 two different Kriging models, namely Ordinary Kriging and Universal Kriging, with a geolithological map of Italy
16 categorized in isotope classes as external predictor. Model performances were evaluated through a 10-fold cross
17 validation, yielding accurate $^{87}\text{Sr}/^{86}\text{Sr}$ predictions with root mean squared errors (RMSE) ranging between 0.0020
18 and 0.0024, dependent on the Kriging model and the sample class. Overall, the produced maps highlight a
19 heterogeneous distribution of the $^{87}\text{Sr}/^{86}\text{Sr}$ across Italy, with the highest radiogenic values (>0.71) mainly localized
20 in three areas, namely the Alps (Northern Italy), the Tuscany/Latium (Central Italy) and Calabria/Sicily
21 (Southern Italy) magmatic/metamorphic terrains. The rest of the peninsula is characterized by values ranging
22 between 0.707 and 0.710, mostly linked to sedimentary geological units of mixed nature. Finally, we took
23 advantage of the case study of Fratta Polesine, to underscore the importance of choosing appropriate samples
24 when building the local isoscape and of exploring different end-members when interpreting the local Sr isotope
25 variability in mobility and provenance studies. Our user-friendly maps and database are freely accessible through
26 the Geonode platform and will be updated over time to offer a state-of-the-art reference in mobility and
27 provenance studies across the Italian landscape.

28 **Keywords:** $^{87}\text{Sr}/^{86}\text{Sr}$ ratio; Kriging; isotope map; spatial modelling; traceability.

29 1. Introduction

30 *Geology is biological destiny: Whatever minerals land or are deposited in a place determine what or who can make*
31 *a living there millions of years later.*

32 (Dennis Overby 2021, New York Times)

33 The provenance of foods, artifacts, animals and individuals is a central topic in archaeology, ecology, forensic
34 science and even in social sciences and humanities. A broad range of methods from genetics to inorganic chemistry
35 can be used to disentangle the geographical origin or the movement of goods/people across the landscape,
36 depending on the nature of the material itself (see e.g. Gregoricka, 2021; Tommasini et al., 2018). Isotope
37 fingerprinting is applied to a variety of samples (e.g. biological tissues, artifacts, rocks, waters) using various isotope
38 systematics of elements such as oxygen (e.g. Pellegrini et al., 2016; Pederzani and Britton, 2019), hydrogen (e.g.
39 Soto et al., 2013), lead (e.g. Vautour et al., 2015; Smith et al., 2019; Killick et al., 2020), strontium (e.g. Bentley,
40 2006), and sulphur (e.g. Bataille et al., 2021) targeting the different materials depending on the element abundance
41 in the sample and the geobiological process under investigation. In this sense, the radiogenic strontium ratio
42 ($^{87}\text{Sr}/^{86}\text{Sr}$) is an excellent tracer of low temperature terrestrial processes for the abundance of elemental Sr and its
43 mobility between the bio-, geo-, and hydro-spheres. While ^{87}Sr is the radiogenic-daughter of ^{87}Rb , ^{86}Sr is stable.
44 Since both strontium and rubidium are ubiquitously present as trace elements within the Earth's crust, crustal
45 rocks will thus acquire different $^{87}\text{Sr}/^{86}\text{Sr}$ ratios in relation to their age and to their initial Sr and Rb contents (Faure
46 and Mensing, 2005). Ultimately, this results in a high-variability of the $^{87}\text{Sr}/^{86}\text{Sr}$ across the landscape (see e.g.
47 Voerkelius et al., 2010). From the bedrock, Sr is transferred to soil, where it mixes with different local pools as
48 surface waters, groundwaters and atmospheric depositions (Bentley, 2006). This is also why 'bioavailable' Sr (i.e.
49 biologically available) might be isotopically different from the bedrock reservoir. In addition, the contribution of
50 different minerals to the soil pool is variable due to i.e. differential weathering, Sr/Rb content and solubility (Sillen
51 et al., 1998). For example, the contribution of Sr-rich carbonates to the local bioavailable reservoir is much larger
52 than e.g. a more resistant to weathering Sr-rich silicate.

53 Sr ions exchanges at the Earth surface carry the isotopic fingerprint shaped over time by the radioactive decay of
54 ^{87}Rb and transfer certain isotopes proportions from rocks to soils and waters. From the soil and water, Sr ions
55 enter the ecosystem reaching plants, through root uptake, and animals, through food and drinking water (Capo

56 et al., 1998). In vertebrates, Sr is then mainly fixed in the hydroxyapatite of tooth and bone tissues substituting
57 calcium (Pors Nielsen, 2004). Across this pathway, mass-dependent Sr isotopic fractionation, as shown by e.g. the
58 relative depletion of the stable $^{88}\text{Sr}/^{86}\text{Sr}$ ratio along the food chain, is likely to occur (Knudson et al., 2010).
59 However, the fractionation of the $^{87}\text{Sr}/^{86}\text{Sr}$ ratio is deemed to be negligible and, anyhow, corrected during mass
60 spectrometry analyses as constant normalization to an internationally accepted ratio (Ehrlich et al., 2001).

61 Sr isotope data from biological samples of interest can be then compared with the local bioavailable Sr isotope
62 ratio in order to understand whether the tissue formed locally or in a geologically different place, tracking the
63 movements of people and goods through space and time (Ericson, 1985; Slovak and Paytan, 2012). Therefore, the
64 subsequent step is to pin-point (more or less precisely) the specific geographic origin of the sample. In this sense,
65 comparison with (inter)national geological maps can help to track the provenance of tissues formed on substrate
66 whose isotopic ratio can be somehow predicted or expected, as for example in old metamorphic crystalline
67 basements (i.e. highly radiogenic Sr isotope values) or depleted mantle-derived magmatic areas (low radiogenic Sr
68 isotope values). Yet, a step-forward in isotope fingerprinting is the building of comparative isotopic maps that
69 show the spatial distribution of the isotope signature (Bowen, 2010).

70 Using patchily-distributed measures of environmental samples, it is possible to build spatial models able to predict
71 the local bioavailable $^{87}\text{Sr}/^{86}\text{Sr}$ ratio of a specific area. These data are then modelled through geostatistic tools in
72 order to predict at best the $^{87}\text{Sr}/^{86}\text{Sr}$ ratio of areas with no available data. The resulting prediction maps are known
73 as isoscapes. The utility of such implements has been demonstrated in several fields and they are today largely
74 employed in provenance studies, as baselines for tracking the provenance of unknown specimens (e.g. Hobson et
75 al., 2010; Muhlfield et al., 2013; Song et al., 2014; Chesson et al., 2018; Colleter et al., 2021; Lazzarini et al., 2021).
76 So far, national isoscapes have been produced for several European and extra-European countries, employing and
77 testing several different methods for the spatial interpolation, including machine learning (Montgomery et al.,
78 2006; Evans et al., 2010; Frei and Frei, 2011; Bataille and Bowen, 2012; Pestle et al., 2013; Hartman and Richards,
79 2014; Copeland et al., 2016; Kookter et al., 2016; Laffoon et al., 2017; Bataille et al., 2018; Hedman et al., 2018;
80 Willmes et al., 2018; Adams et al., 2019; Ladegaard-Pedersen et al., 2020; Scaffidi and Knudson, 2020; Snoeck et
81 al., 2020; Wang et al., 2020; Frank et al., 2021; Funck et al., 2021; Washburn et al., 2021; Zieliński et al., 2021).
82 Although a large amount of 'bioavailable' Sr data was produced in the past, mostly linked to food provenance and
83 archaeological studies, a national isoscape for Italy is still lacking. A first attempt has been done by Emery et al.

84 (2018), where an inverse distance weighting (IDW) interpolation was tested using some literature data to produce
85 a preliminary Italian isoscape.

86 Here, we extended the database presented by Emery et al. (2018), using both novel and published data, and we
87 performed a robust geospatial modelling, employing Ordinary Kriging and Universal Kriging (Willmes et al.,
88 2018). Kriging is a widely used regression method in geostatistics and is based on the principle of ‘spatial
89 autocorrelation’ (Krige, 1951). This consists in best-fitting a mathematical function (i.e. variogram) to a
90 predetermined number of points with the aim of determining the output value for unknown locations and thus
91 generating a continuous surface map (Oliver and Webster, 1990). We produced maps of Italy exploiting the
92 Kriging methods and using an extensive dataset, which includes both ‘bioavailable’ and ‘non-bioavailable’ Sr
93 isotope values (available at geochem.unimore.it/sr-isoscape-of-italy). The latter integrates bulk rock values from
94 magmatic and metamorphic rocks. We acknowledge that to understand the provenance of biological samples, the
95 best approach is to compare their isotopic fingerprint to bioavailable Sr isotope data. However, the inclusion of
96 sparse rock values allowed us to understand the ‘weight’ of the bedrock influence on the local Sr isotope
97 composition in specific areas of Italy. For this reason, we ultimately generated two maps, one with exclusively
98 bioavailable data and one that includes all the values from the dataset. Maps are freely accessible at
99 geochem.unimore.it/sr-isoscape-of-italy, through the GeoNode platform (geonode.org).

100

101 2. Data and methods

102 2.1 Sample selection

103 Strontium isotope data were collected ($n = 1831$) from the literature (60 manuscripts) and categorized by source
104 in six different clusters (Figure 1), namely ‘plant’, ‘water’, ‘biomineral’ (i.e. bones, teeth and bio-calcareous shells),
105 ‘food’, ‘soil’ (including both exchangeable soil fractions and bulk soils) and ‘rock’ (mainly evaporites,
106 metamorphic and magmatic rocks, and a few sedimentary bulk rocks). For each group, descriptive statistics
107 analyses (i.e. mean, standard deviations and quantiles) were performed using Origin v. 2020 (see Table 1). We
108 incorporated in our dataset both bioavailable and non-bioavailable (namely rocks and bulk soils) Sr isotope data
109 and generated two maps (see below): one including the sole ‘bioavailable’ data and one including ‘all’ data

110 ('bioavailable' + 'non-bioavailable'; see Table S1). This allowed us to obtain a broader overview of the Sr isotope
 111 distribution across Italy.

Table 1. Descriptive statistics for the different sample categories.

Category	N total	Mean	2 SD	Minimum	Median	Maximum	Interquartile Range (Q3 - Q1)
Plant	72	0.70881	0.00117	0.70778	0.70867	0.71122	0.00069
Water	476	0.71005	0.01013	0.70354	0.70887	0.76384	0.00120
Biominerals	471	0.70872	0.00182	0.70729	0.70866	0.71614	0.00094
Food	296	0.70926	0.00282	0.70679	0.70899	0.72071	0.00071
Soil	273	0.70994	0.00549	0.70528	0.7091	0.72379	0.00131
Rock	332	0.71064	0.01081	0.70319	0.70898	0.753	0.00212
Whole dataset ('all')	1920	0.70964	0.00734	0.70319	0.70888	0.76384	0.00105

112
 113 Novel data (n = 89) were generated from modern environmental and archaeological samples by solution MC-
 114 ICPMS analyses. Samples include modern vegetation, archaeological and modern teeth, snails, waters, rocks and
 115 soils. These samples are from areas where archaeological studies are in progress and thus were integrated into the
 116 database. Five meteoric water samples collected from pluviometers located in the Emilian Apennine
 117 (Montecagno, 44°19'57.76" N; 10°21'58.57" E) were also measured for their Sr isotopic composition. These values
 118 were not included in the spatial model, but are presented as possible end-members for the Sr cycle in the biosphere,
 119 possibly helpful for future studies on Sr mixing (Table 2).

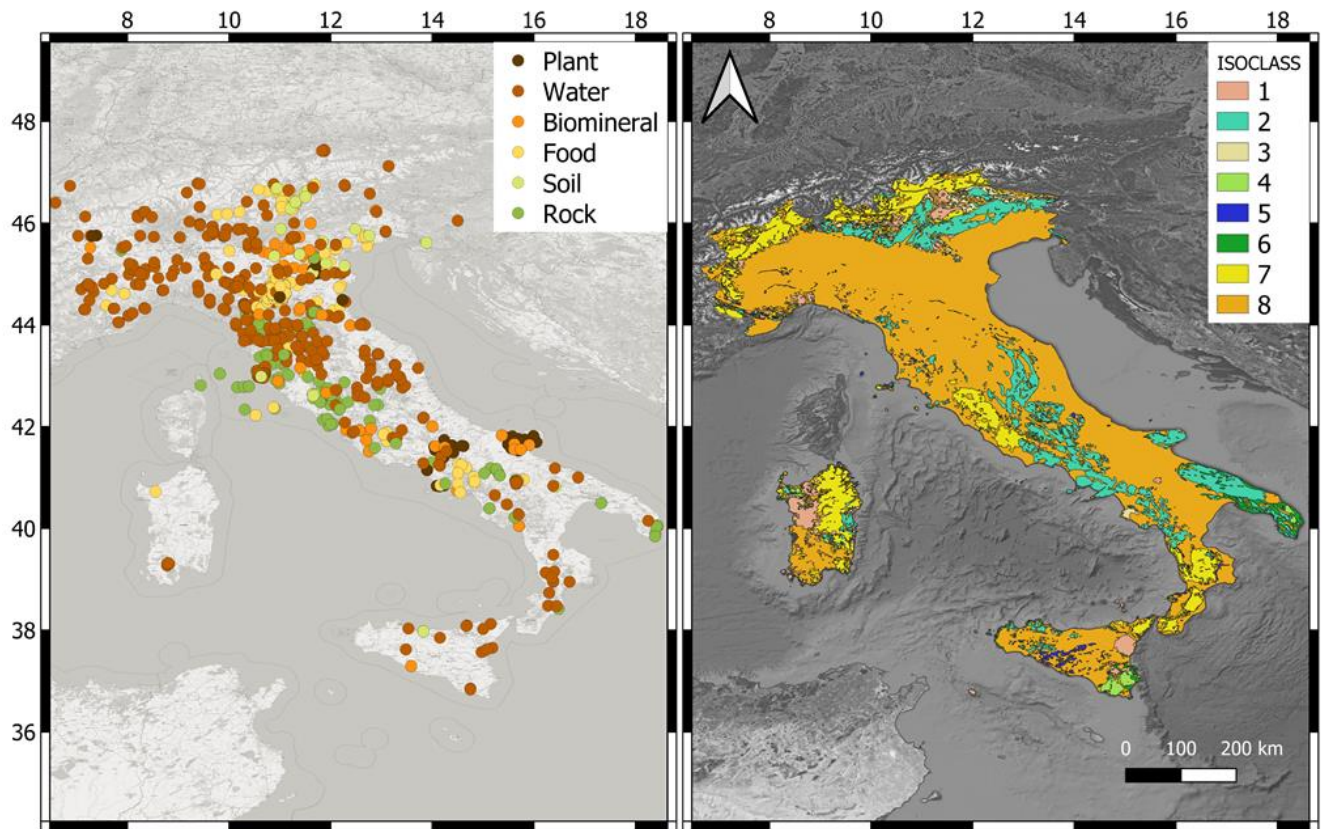
Table 2. Sr isotopes of meteoric waters measured in this study.

Latitude	Longitude	Sampling date	Material	⁸⁷ Sr/ ⁸⁶ Sr	2 SE
44°19'57.76" N	10°21'58.57" E	March 2016	Meteoric water	0.70848	0.00001
44°19'57.76" N	10°21'58.57" E	June 2016	Meteoric water	0.70873	0.00001
44°19'57.76" N	10°21'58.57" E	October 2016	Meteoric water	0.70882	0.00001
44°19'57.76" N	10°21'58.57" E	March 2017	Meteoric water	0.70924	0.00001
44°19'57.76" N	10°21'58.57" E	July 2017	Meteoric water	0.70897	0.00001

121 2.2. Solution MC-ICPMS

122 Samples were processed at the Geochemistry Lab of the Department of Chemical and Geological Sciences
 123 (University of Modena and Reggio Emilia) and at Durham University. All the reagents employed were of suprapur
 124 grade (Modena) or bidistilled (Durham). Biominerals (i.e. teeth and snail shells) were cleaned with MilliQ water
 125 and digested using concentrated HNO₃. The bioavailable Sr fraction from soils instead was extracted using 0.25M
 126 acetic acid. Bulk rocks samples were totally digested using a mixture of concentrated HNO₃ and HF. Waters were
 127 filtered and acidified with HNO₃ to a concentration of 3M. After drying and re-dissolution by 3M HNO₃, all
 128 samples were processed using the Eichrom Sr-spec resin. The ⁸⁷Sr/⁸⁶Sr ratios were determined by Neptune MC-
 129 ICPMS, one housed at the Centro Interdipartimentale Grandi Strumenti of the University of Modena and Reggio

130 Emilia and one at the Northern Centre for Isotopic and Elemental Tracing at Durham University. Detailed
131 protocols are described in Lugli et al. (2017), Argentino et al. (2021) and Cavazzuti et al. (2019a, b). Repeated
132 measures of NBS987 yielded an $^{87}\text{Sr}/^{86}\text{Sr}$ value of 0.710237 ± 0.000011 (2 SD; n = 18; Modena) and $0.710267 \pm$
133 0.000014 (2 SD; n = 57; Dhuram). All values were reported to an NBS987 accepted value of 0.710248 (McArthur
134 et al., 2001).



135
136 Figure 1. Left panel: locations of the data points considered in this study. Most of the data are from literature, with the
137 addition of novel unpublished environmental/archaeological samples. All the samples in the ‘plant’, ‘water’, ‘biomineral’ and
138 ‘food’ categories are considered ‘bioavailable’, in addition to ‘soil’ leachates. ‘Rock’ and bulk ‘soil’ are considered ‘non-
139 bioavailable’. This map was built in QGIS 3.8, exploiting the OpenStreetMap service. Right panel: Isoclass map of Italy that
140 is a map of the Italian geolithologies classified according to their expected isotope values. This map is based on the
141 geolithological map of Italy available at the Geoportale Nazionale
142 (http://wms.pcn.minambiente.it/ogc?map=/ms_ogc/wfs/Carta_geolitologica.map); the satellite map is provided by Google
143 through the QGIS QuickMapServices plug-in. Isoclass 1: plutonic and volcanic rocks related to MORB mantle magmatism
144 of different ages. Isoclass 2: marine carbonate rock formations of Late Triassic, Cretaceous and Jurassic ages. Isoclass 3: Early
145 and Middle Triassic and Paleogenic marine carbonate rocks. Isoclass 4: Early and Medium Miocene marine carbonate

146 formations. Isoclass 5: Late Miocene carbonates. Isoclass 6: Pleistocene and Pliocene carbonate formations. Isoclass 7: old
147 metamorphic and magmatic rocks of the crystalline basement and younger volcanics whose magmatism is affected by a
148 radiogenic Sr isotope source. Isoclass 8: all the geolithologies not attributed to an isotope class due to their hybrid nature (i.e.
149 siliciclastic rocks) or to their large Sr isotope variability (i.e., Permian to Devonian carbonates have a very wide range of Sr
150 isotope ratios across several of our defined classes).

151

152 2.3 Geospatial modelling

153 All the identified literature data and new data were grouped in an Excel worksheet and imported into SAGA 7.9
154 for geospatial modelling. We employed two different models to obtain the interpolated $^{87}\text{Sr}/^{86}\text{Sr}$ maps, namely
155 Ordinary Kriging and Universal Kriging. The latter is drifted using a geological map of Italy as auxiliary predictor,
156 similarly to the Kriging model with external drift of Willmes et al. (2018). However, unlike Willmes et al. (2018),
157 where the isotope groups were defined using clustering techniques on the data itself, we relied on a simplified
158 geological map of Italy (Figure 1), generated *ad hoc* for this project, combining geolithologies and expected isotope
159 values of the rock formations. In particular, we defined eight isotope classes ('isoclass', Figure 1) taking advantage
160 of: 1) the expected Sr isotope range of certain rock formations outcropping in the Italian peninsula as reported in
161 the literature; 2) the categorization of geological units (i.e. metamorphic, magmatic, sedimentary, etc.) of the
162 Italian geolithological map (published by the Geoportale Nazionale, pcn.minambiente.it; see also Figure S1); 3)
163 the Sr isotope seawater curve of McArthur et al (2001), which in Italy finds wide application due to the continuous
164 marine carbonate deposits from the Triassic to the Neogene preserved across the peninsula. Notably a relatively
165 high number of isotope data is available in the literature for metamorphic and magmatic rocks across Italy, which
166 have been measured to understand the geodynamic events that led to the formation of the Alps and Apennines
167 and their emplacement at crustal level. Although most of these data were not included in the database, because no
168 geolocalization was available, their isotope signature was used to define isoclasses as building blocks of the Italian
169 Sr isomap. In addition, several published Sr isotope data were measured on single mineral phases and therefore,
170 being not representative of the bulk rock, could not be used for our purpose.

171 The range of Sr isotope values of the eight isoclasses is defined as follows: Isoclass 1 (expected $^{87}\text{Sr}/^{86}\text{Sr} < 0.70682$)
172 includes plutonic and volcanic rocks related to MORB mantle magmatism of different ages. Isoclass 2 ($0.70682 <$
173 $\text{expected } ^{87}\text{Sr}/^{86}\text{Sr} < 0.70783$) includes mainly marine carbonate rock formations of Late Triassic, Cretaceous and
174 Jurassic ages. Isoclass 3 ($0.70783 < \text{expected } ^{87}\text{Sr}/^{86}\text{Sr} < 0.70825$) includes Early and Middle Triassic and Paleogenic

175 marine carbonate rocks. Isoclass 4 ($0.70825 < \text{expected } ^{87}\text{Sr}/^{86}\text{Sr} < 0.70885$) includes Early and Medium Miocene
176 marine carbonate formations. Isoclass 5 ($0.70885 < \text{expected } ^{87}\text{Sr}/^{86}\text{Sr} < 0.70903$) includes mainly Late Miocene
177 carbonates. Isoclass 6 ($0.70903 < \text{expected } ^{87}\text{Sr}/^{86}\text{Sr} < 0.70920$) includes Pleistocene and Pliocene carbonate
178 formations. Isoclass 7 ($\text{expected } ^{87}\text{Sr}/^{86}\text{Sr} > 0.70920$) includes old metamorphic and magmatic rocks of the
179 crystalline basement and younger volcanics whose magmatism is affected by a radiogenic Sr isotope source. Isoclass
180 8 finally includes all the geolithologies that we were not able to attribute to an isotope class due to their hybrid
181 nature (i.e. siliciclastic rocks) or to their wide Sr isotope variability (i.e., Permian to Devonian carbonates have a
182 very wide range of Sr isotope ratios across several of our defined classes).

183 In attributing the isoclass to a particular geolithology or formation we confronted local rock values from literature
184 and, whenever possible, double checked their consistency with the bioavailable values of our database. When no
185 data were available, we considered the type of rock (i.e. mineralogy) and the age of formation. Initially, we defined
186 several more isoclasses in the Sr isotope range especially in the range between 0.7092 and very radiogenic values
187 (up to 0.75). However, we could attribute with certainty only a few data points from Sardinia to these classes, and
188 therefore we finally grouped all Sr isotope ratios > 0.7092 in a unique class (isoclass 7). We stress that the
189 attribution of an isoclass has not been arbitrary and any attribution is either backed up by isotopic data or
190 consistent with a particular type of magmatism or deposition event (e.i. seawater curve for marine carbonates of
191 McArthur et al., 2001).

192 For geospatial modelling, the observed variograms were fit through a linear model, with a searching range of ca.
193 180 km. Similarly to what observed by Hoogewerff et al. (2019), the semivariograms obtained here showed a
194 cyclical-like structure, with a first maximum located at approximately 250 km (Figure S2). The prediction power
195 of the models was evaluated using a 10-fold cross-validation method through SAGA 7.9 (Table 3). The
196 interpolated Kriging models were imported into QGIS 3.18 to generate the final distribution maps (freely available
197 online at geochem.unimore.it/sr-isoscape-of-italy). We note here that Sardinia was excluded from the Ordinary
198 Kriging due to the low number of data from the area.

Table 3. 10-fold cross validation results for Kriging model performances through SAGA 7.9.

Model	Dataset	N. data points	RMSE	Normalized RMSE (%)	R ² (%)
Ordinary Kriging	'bioavailable'	1568	0.0021	3.5	59.5
	'all'	1920	0.0024	3.9	66.0
Universal Kriging	'bioavailable'	1568	0.0020	3.4	59.0
	'all'	1920	0.0022	3.6	69.7

199

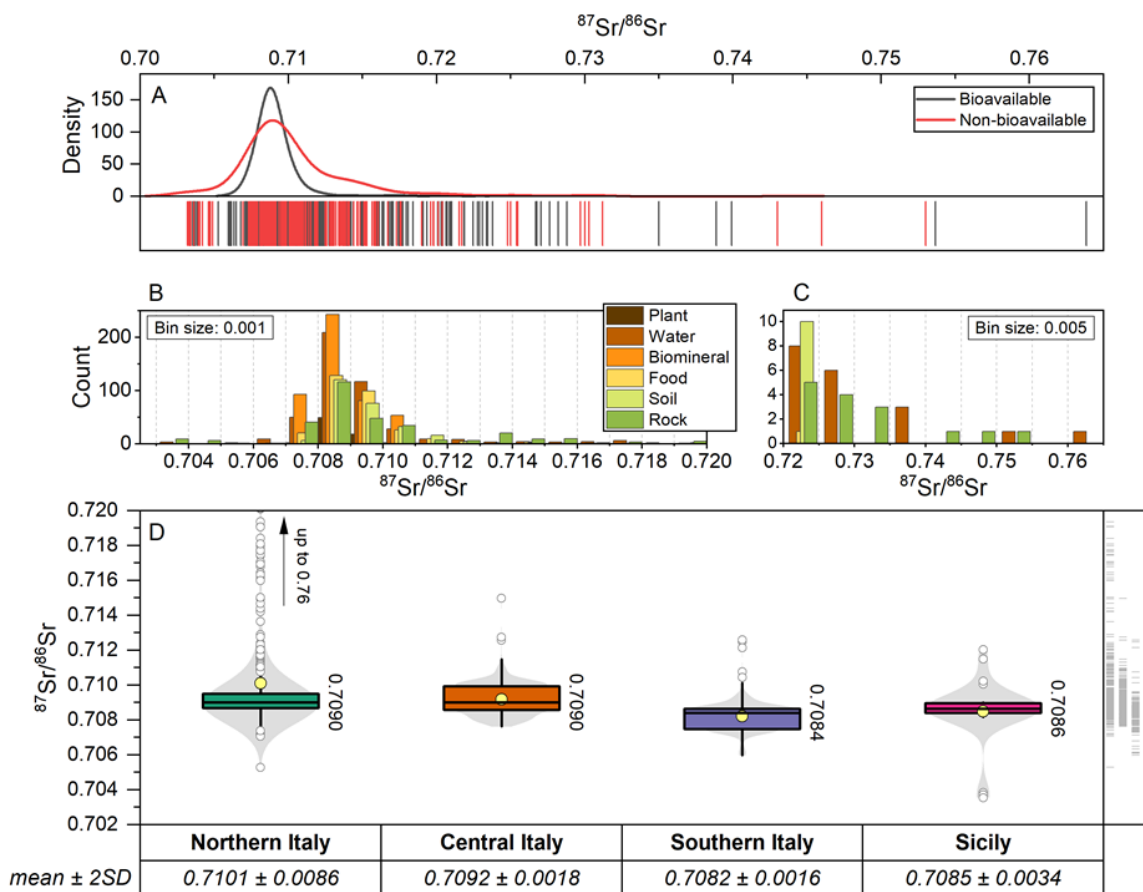
200 3. Results and discussion

201 3.1. Data description and distribution

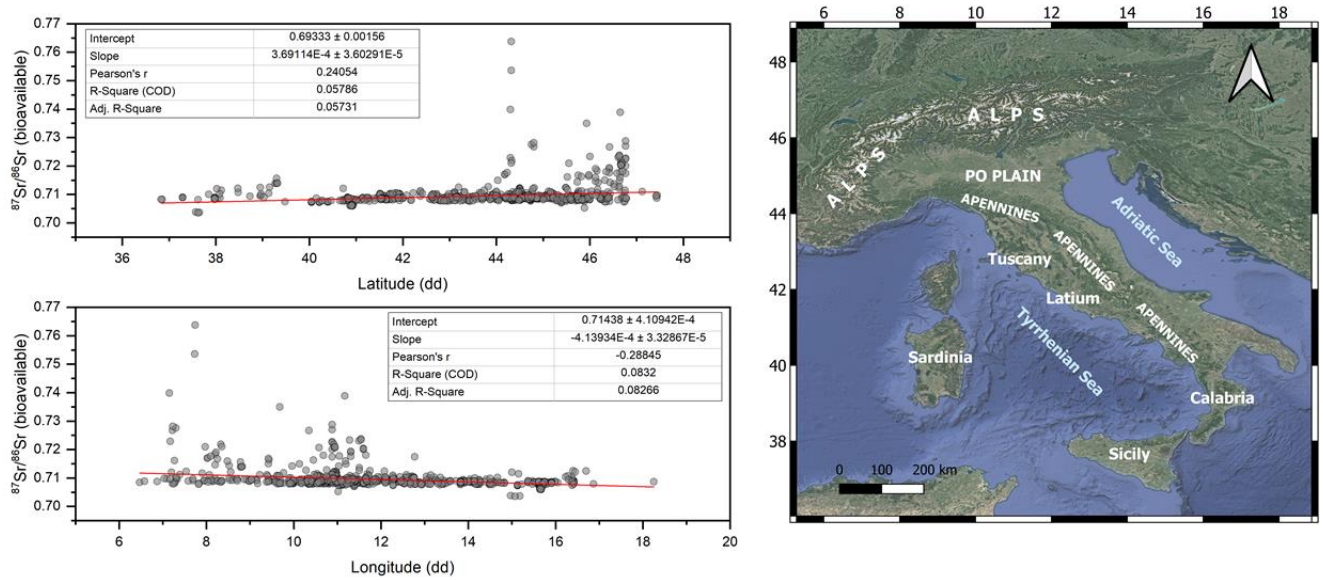
202 Descriptive statistics for the data considered in this study are reported in Tables 1 and S1 and summarized in
203 Figures 2 and S3. When categorized, the ‘rock’ group has as expected the larger variance of the whole dataset, with
204 a $^{87}\text{Sr}/^{86}\text{Sr}$ ranging from 0.70319 to 0.75300 (Figure 2). This group also shows the averagely highest Sr isotope
205 values (0.7106). On the contrary, plants and biominerals are characterized on average by the lowest Sr isotope
206 values (0.7087-0.7088). The most extreme values of the dataset are found within ‘rock’ (0.70319) and ‘water’
207 (0.76384) groups (see Table 1). Bioavailable samples show an average $^{87}\text{Sr}/^{86}\text{Sr}$ ratio of 0.70941 ± 0.00632 (2 SD),
208 and span between 0.70354 and 0.76384, with a median value of 0.70883. The kernel density distribution of the
209 bioavailable data is strongly asymmetric and leptokurtic (skewness = 8.14; kurtosis = 99.16). Notably, the non-
210 bioavailable samples, including all the rocks and bulk soils, display an average $^{87}\text{Sr}/^{86}\text{Sr}$ ratio of 0.71069 ± 0.01054
211 (2 SD), ranging between 0.70319 and 0.75300, with a median value of 0.70900 (Table S1). The distribution of
212 the non-bioavailable dataset is asymmetric but less leptokurtic than the bioavailable (skewness = 3.93; kurtosis =
213 22.40). Yet, we stress that the number of non-bioavailable data ($n = 352$) here considered is remarkably lower than
214 the data in the bioavailable dataset ($n = 1568$), potentially influencing our observations on the data. Similarly, the
215 uneven spatial distribution of ‘non-bioavailable’ samples across Italy certainly influenced data evaluations and use
216 for this class. $^{87}\text{Sr}/^{86}\text{Sr}$ ratios of the bioavailable samples were also exploratively plotted against latitude and
217 longitude (Figure 3), searching for potential correlations between these variables. However, no statistically
218 significant trend was observed (both $R^2 < 0.1$). Yet, the two graphs clearly show a preferential distribution of the
219 highest radiogenic Sr values northwards (latitude 44-47° N) and eastwards (longitude 7-12° E). This is expected
220 due to the presence of old metamorphic and magmatic rocks in the Alpine area and magmatic-metamorphic
221 provinces in Central Italy (Tuscany, Latium), and also evident when data are plotted by Italian macroregions
222 (Figure 2).

223 Five meteoric waters, not included in the previous statistics evaluations (and the interpolated maps) range between
224 0.70848 and 0.70924, and represent an end-member of the Sr bioavailable cycle. These five waters were sampled
225 from the same pluviometer located in the Emilian Apennine, and they were seasonally collected ca. 3-to-5 months
226 apart from each other. These data highlight a remarkable temporal variability of the local rainwater likely due to

227 the changing contribution of seawater aerosol and crustal dust, with a possible important influence on the local
 228 bioavailable Sr (Négrel et al., 2007).



229
 230 Figure 2. Data exploration. A) Kernel density estimation of bioavailable (n = 1568) vs. non-bioavailable (n = 352) $^{87}\text{Sr}/^{86}\text{Sr}$
 231 data. B) Superimposed histogram representing the different sample categories between 0.702 and 0.720, with a bin size of
 232 0.001. C) Superimposed histogram of the different sample categories between 0.720 and 0.77, with a bin size of 0.005. Note
 233 that the y-scale ranges of the histograms ('count') are different. D) Sr isotope data grouped by geographical areas
 234 (macroregions) of Italy, defined according to the National Institute of Statistics (istat.it); median values are labelled close to
 235 the box plots; average values $\pm 2\text{SD}$ are also reported.

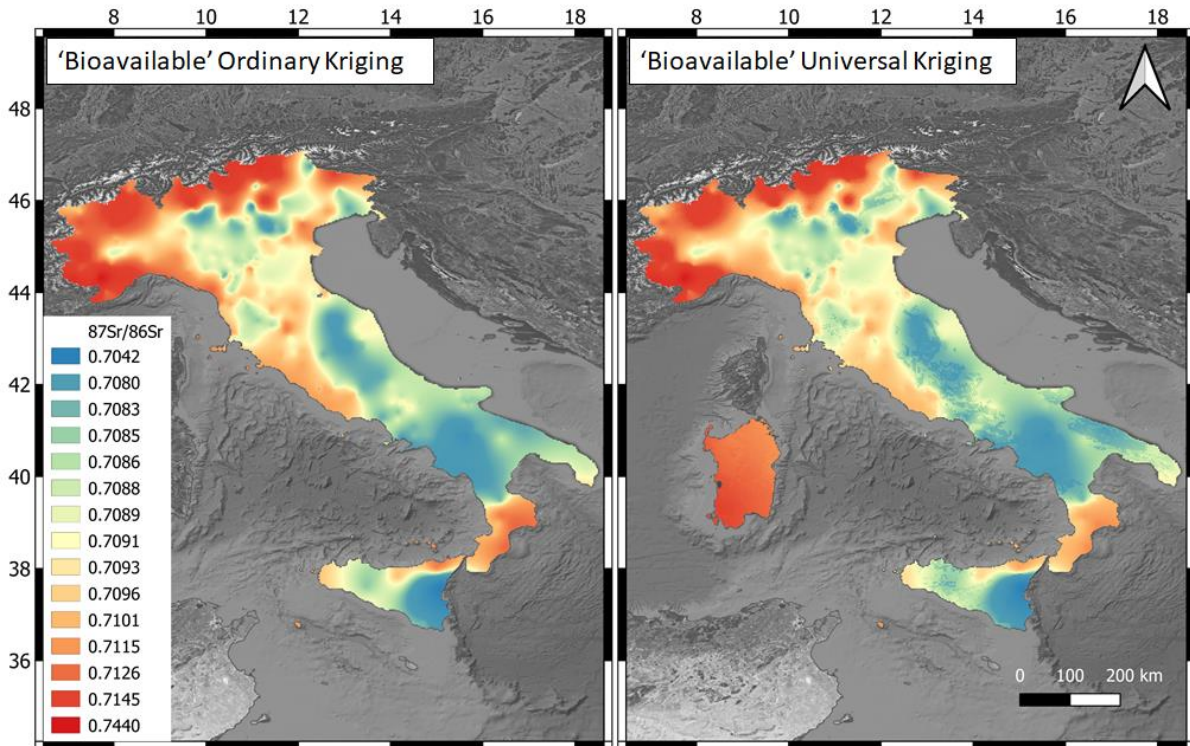


236
 237 Figure 3. The $^{87}\text{Sr}/^{86}\text{Sr}$ ratios plotted against latitude and longitude (decimal degrees). No significant linear trend appears;
 238 however, most of the radiogenic Sr data are latitudinally distributed northwards and longitudinally eastwards. Graphs and
 239 linear trends were produced using Origin v. 2020. Right panel: a geographic map of Italy is reported as reference; main areas
 240 cited in the manuscript are labelled.

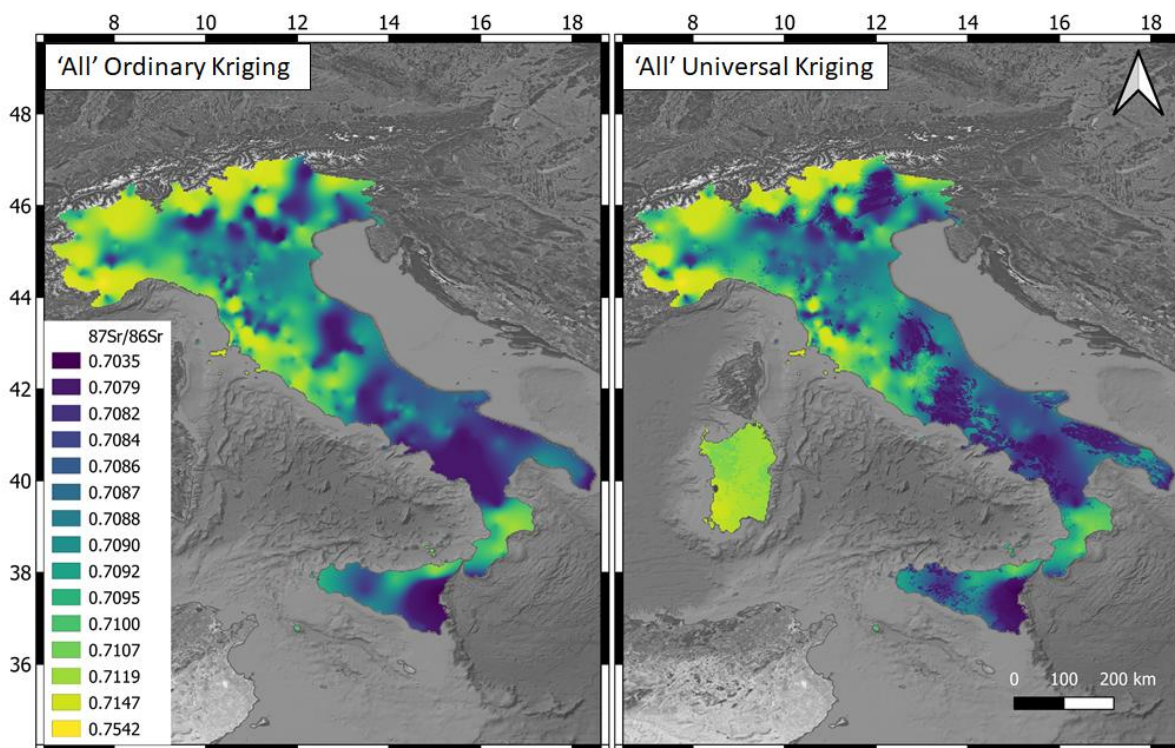
241
 242 3.2. Maps

243 The isoclass map of Italy (Figure 1) allows a first order distinction between the radiogenic Sr isotope provinces,
 244 related to the ‘old’ crustal and radiogenic Sr isotope magmatism units mainly present in the Alps, Calabria,
 245 Sardinia and Central Italy, and the unradiogenic provinces related to the depleted mantle magmatism mainly in
 246 the Southern Alps and Sicily. Yet, more information can be gathered through the isoscape maps (Figures 4 and 5).
 247 These were built modelling the two datasets, namely ‘bioavailable’ and ‘all’. Each figure includes two maps
 248 obtained with two distinct Kriging approaches: Ordinary and Universal with external drift. The evaluation of
 249 performance of the two models is reported in Table 3. Both methods produced satisfying results, with relatively
 250 low normalized root mean squared errors (NRMSE \sim 3-4%), explaining between \sim 60 and \sim 70% of the isoscape
 251 variance (R^2). In general, Universal Kriging (with external drift) seems to outperform Ordinary Kriging, although
 252 the difference is not remarkable (Table 3). The lowest RMSE is observed for the ‘bioavailable’ Universal Kriging,
 253 and is equal to 0.0020; instead, the highest RMSE (0.0024) was obtained for the ‘all’ Ordinary Kriging model.
 254 Altogether, the presence of non-bioavailable (un)radiogenic end-members in the ‘all’ database seems to limit the

255 prediction power of the Kriging method, both in terms of data over-fitting (higher R^2) and worse variogram
256 modelling (see also Figure S4). To further evaluate the prediction of our modelling we measured the prediction
257 standard errors for the Kriging maps (Figure S4). Both models (i.e. Ordinary and Universal) show similar standard
258 prediction errors, ranging from ca. $5E-7$ to $5E-6$ for the ‘bioavailable’ dataset and from $2E-7$ to $2E-5$ for the ‘all’
259 dataset. These errors are low when compared with other spatial interpolation presented in literature for isoscapes
260 (e.g. Willmes et al., 2018; Adams et al., 2019; Wang et al., 2020). Such low values are possibly related to the high
261 number of samples considered in this study (total $n = 1920$), evenly distributed across Italy (see Figure 1),
262 compared to the available literature studies. Largest errors indeed can be found in Sicily and Sardinia, where the
263 number of samples is significantly lower than in other areas (Figure S4).



264
265 Figure 4. Ordinary and Universal (with external drift) kriging models obtained for the ‘bioavailable’ $^{87}\text{Sr}/^{86}\text{Sr}$ dataset. Maps
266 were obtained using SAGA 7.9 and QGIS 3.8.



267
268 Figure 5. Ordinary and Universal (with external drift) kriging models obtained for the 'all' $^{87}\text{Sr}/^{86}\text{Sr}$ dataset. Maps were
269 obtained using SAGA 7.9 and QGIS 3.8.

270
271 The 'bioavailable' (Figure 4) and the 'all' (Figure 5) maps show similar spatial distribution of the $^{87}\text{Sr}/^{86}\text{Sr}$ ratios,
272 with the highest radiogenic values clustered in well-defined geological areas of Italy, namely the Alps, the Tuscan
273 Magmatic Province, the Latium volcanic area and the Calabria crystalline basement (Southern Italy). These values
274 are of course related to the radiogenic nature of the natural components from these areas included in our database.
275 Contrariwise, low Sr isotope values are generally present in areas characterized by depleted mantle magmatism
276 such as in Sicily and in Campania and where old carbonates (older than Pliocene) outcrop.

277 The largest differences in terms of isoscape predicted values among the 'all' and the 'bioavailable' maps arise indeed
278 in these areas (particularly Tuscany and Latium), due to the presence of even higher radiogenic values in local
279 rocks, only partially identified in the bioavailable pool (see Figure S5). The north-western Alpine area also shows
280 significant differences (both in negative and positive) between the two datasets. However, here, only few rock
281 values are present within the 'all' database. This suggests that the observed variations (see e.g. Cuneo area, north-

282 western Italy) are probably linked to model's predictions inaccuracies rather than actual variations of the $^{87}\text{Sr}/^{86}\text{Sr}$
283 ratio.

284 Overall, several small 'hotspots' (both negative and positive) can be recognized when comparing the predictions
285 of the two datasets, particularly in the Alps. We stress that the number of samples in these areas is lower than in
286 other localities; however, another explanation might lie in the complex geometry of the Alps where the
287 bioavailable Sr isotope ratios might differ from those of the exposed rocks because of the geological complexity of
288 the nappes that overthrust each other in the belt and therefore in the differential contributions to the bioavailable
289 Sr possibly from other reservoirs.

290 Sharper details of the isotope zones can be observed in the Universal Kriging map compared to the Ordinary
291 Kriging, due to the definite isoclass boundaries of the guiding map. In general, when looking at specific areas of
292 the map, the Universal Kriging model should be more accurate in terms of spatial prediction, particularly for those
293 areas with few data available. However, the Ordinary Kriging map seems to better mimic the natural averaging of
294 Sr isotope values due to weathering and mixing processes.

295

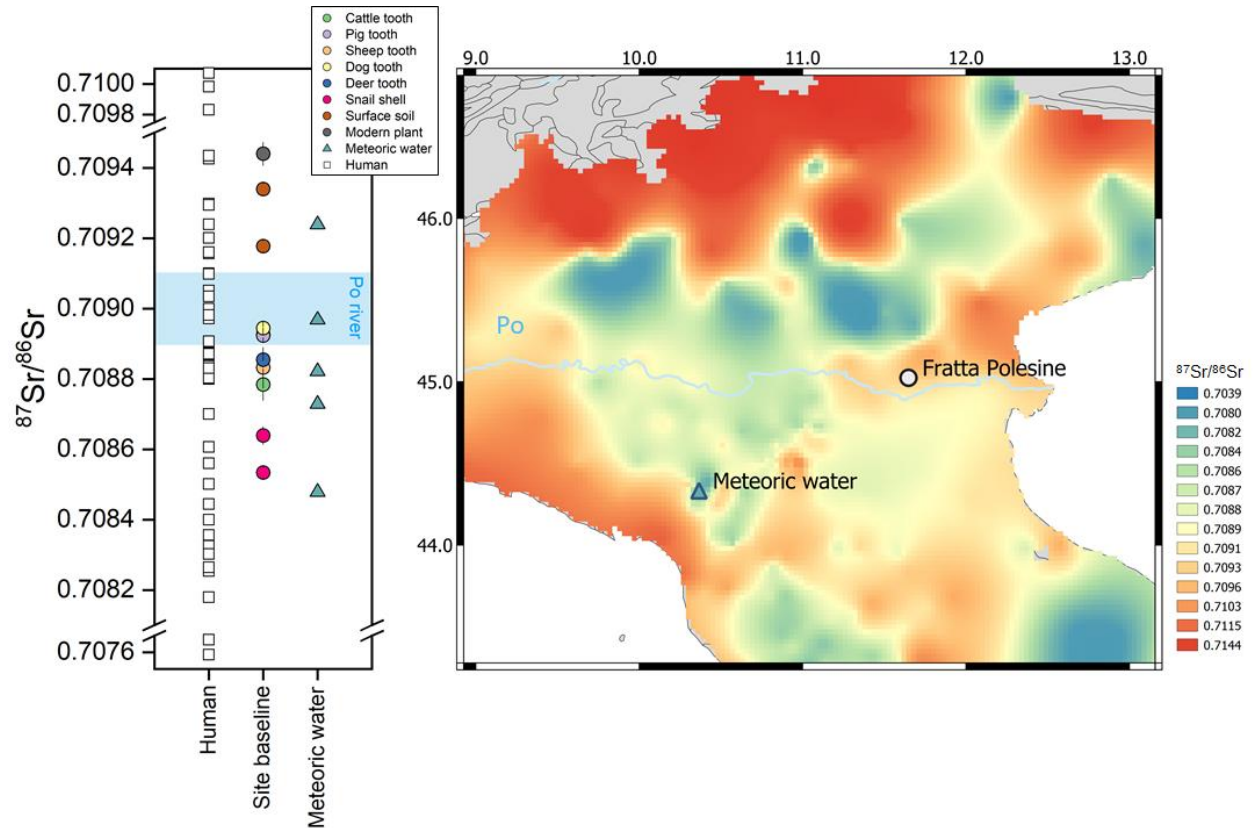
296 3.3. Definition of the local bioavailable Sr baseline for human provenance: a case study

297 Defining the local bioavailable Sr baseline is currently a hot topic in archaeology and anthropology. Common
298 methods include the measurement of modern environmental samples as waters, plants, snail shells and soil
299 leachates (Bentley, 2006; Maurer et al., 2012; Ladegaard-Pedersen et al., 2020; Toncala et al., 2020), but also
300 through the analysis of local (archaeological) fauna (see e.g. Lugli et al., 2019). Some studies also showed the power
301 of using statistical methods to detect outliers (as Tukey's fences and median absolute deviations) among the
302 human's skeletal isotopic dataset, to constrain local vs. non-local individuals (Lightfoot and O'Connell, 2016;
303 Cavazzuti et al., 2021). Once defined, the local baseline is then used to comprehend the mobility patterns of the
304 investigated human population (i.e. autochthonous vs. allochthonous individuals). However, there is no general
305 consensus on the best practices to employ for determining the local Sr baseline (e.g. Maurer et al., 2012; Britton et
306 al., 2020; Weber et al., 2021). All the methods have indeed intrinsic flaws linked to various sources of error such
307 as anthropogenic contaminations on environmental samples (Thomsen and Andreasen, 2019), temporal changes
308 in the Sr mixing end-members (e.g. Erel and Torrent, 2010; Han et al., 2019) or simply erroneous *a priori*
309 assumptions. For example, were 'local' animals actually 'local'? What is their real home range? Are modern plants,

310 growing on modern soils, isotopically representative of the ancient landscape? All these are open questions that
311 call for further investigations and can lead to data misinterpretation if not considered.

312 We take advantage of some of the novel data measured for this study to further discuss this issue, focusing on the
313 Bronze Age archaeological site of Fratta Polesine (Cardarelli et al., 2015; Cavazzuti et al., 2019a) in the Po plain
314 (Northern Italy). Locally, the geology is characterized by Holocene alluvial debris, mainly composed of siliciclastic
315 sedimentary deposits related to the erosion of the Alpine belt. We built a bioavailable Sr isoscape excluding the
316 bioavailable data from the site, to compare the Ordinary Kriging interpolated data against the Fratta Polesine
317 measured dataset (Figure 6). The Ordinary Kriging interpolated $^{87}\text{Sr}/^{86}\text{Sr}$ ratio, in a radius of 10 km from the site,
318 ranges between 0.7091 and 0.7096, with a median value of 0.7094. The measured bioavailable data from Fratta
319 Polesine are averagely less radiogenic (0.7089) but more variable, ranging between 0.7085 (snail) and 0.7094
320 (modern shallow rooted plant). These specimens plot as three distinct clusters, with plant and soils showing the
321 highest values (0.7092-0.7094), snails the lowest (0.7085-0.7086), and animal enamel falling in the middle (0.7088-
322 0.7089). Such variability in our measured data suggests that different end-members influenced in different ways
323 the environmental specimens. Plants (mostly shallow rooted plants) and soils are indeed likely to be more
324 influenced by atmospheric deposition and anthropogenic contaminants. Yet, the rainwaters from the Apennines
325 show a maximum value of 0.7092 (Table 2), suggesting that other sources (as dust, fertilizers and/or other antropic
326 sources) might have contributed to the plant-soil pool at Fratta Polesine (Thomsen and Andreasen, 2019). Our
327 isoscape agrees with the presence of higher radiogenic values towards the north-east. Hence, we can alternatively
328 hypothesize that underground waters flowing southwards from the Alps into the Po plain might have influenced
329 the local isotope fingerprint of soils and plants from Fratta Polesine.

330 Snail shells are characterized by the lowest radiogenic $^{87}\text{Sr}/^{86}\text{Sr}$ ratios among the measured samples. This has been
331 observed before in the literature (Maurer et al., 2012; Britton et al., 2020), and linked to the amount of soil
332 carbonate (up to 40%) incorporated into the diet of land snails (Yanes et al., 2008; Maurer et al., 2012). Animal
333 enamel shows intermediate values, possibly reflecting different sources of drinking water and food (Toncala et al.,
334 2020). For example, the (domesticated?) dog and pig teeth are isotopically compatible with the Po river water, one
335 of the main sources of drinking water close to Fratta Polesine. Human data presented in Cavazzuti et al. (2019a)
336 show a median $^{87}\text{Sr}/^{86}\text{Sr}$ ratio of 0.7089, with an interquartile range (Q3-Q1) of 0.0006, indicating that most of
337 the individuals are compatible with the baseline of the site and few plot outside the local environmental variability
338 (see Cavazzuti et al., 2019a for more details).



339
 340 Figure 6. Local baseline at the Bronze Age site of Fratta Polesine (Rovigo, Veneto). Analysed samples include animal tooth
 341 enamel, snail shells, surface soil leachates and vegetation. Human data (including both enamel and cremated petrous bone
 342 specimens) are from Cavazzuti et al. (2019a). In the graph, meteoric water data from the Apennines (blue triangles) and water
 343 data (light blue area) from the Po river (sampling locations close to the site) are reported for comparison. The Sr bioavailable
 344 map on the right panel is an Ordinary Kriging interpolation, without the local data from Fratta Polesine. The local (<10 km)
 345 predicted $^{87}\text{Sr}/^{86}\text{Sr}$ range at the site is 0.7091-0.7096 (median 0.7094). The Po river is also shown on the map.

346
 347 Overall, these data suggest that soils (leachates) and plants best reflect the local bioavailable Sr pool, although
 348 possibly contaminated by modern and/or antropic end-members. Fauna enamel, if truly local as in the case of
 349 domesticated macro-mammals or small home range micro-mammals, mixes various bioavailable Sr sources and
 350 more closely mimics the local food and drinking sources. Such evidence clearly highlights the intrinsic limits in
 351 using isoscapes, which are commonly composed by a patchwork of literature data from different samples, or
 352 modelled on specific samples collected *ad hoc* (as soils or plants). Yet, we stress here that Sr isotopes need to be
 353 interpreted following an ‘exclusion’ principle, and thus employed to *discard* possible areas as point of origin (Holt

354 et al., 2021). This, in turn, suggests that provenancing through isoscapes, and isotope baselines in general, need to
355 be performed with caution. Hence, isoscapes must be considered as ‘guides’ for data interpretation, rather than
356 an unequivocal provenancing tool, justifying their composite nature to better understand the variability of local
357 Sr pools.

358

359 4. Conclusions

360 We collected a large amount of georeferenced Sr isotope values for Italy. Owing to this database, we were able to
361 produce $^{87}\text{Sr}/^{86}\text{Sr}$ prediction maps by geostatistical modelling, namely Ordinary Kriging and Universal Kriging.
362 Model performances were evaluated through 10-fold cross validations, resulting in RMSE ranging between
363 0.0020 and 0.0024.

364 Bioavailable Sr isotope values across Italy show a remarkable variability, with the Alps and certain
365 metamorphic/magmatic terrains displaying the highest radiogenic values, and are in general well-consistent with
366 the underlying bedrock type.

367 We took advantage of the produced maps to discuss a local case study and the definition of local baseline in
368 archaeological studies, a currently hot-topic within the field of provenance and mobility studies. In this sense,
369 regional and (extra)national isoscapes are key in understanding the variability of the local Sr pool, broadening our
370 understanding on the mixing of the different end-members to obtain certain isotope signatures in (geo)biological
371 samples.

372 Distribution maps of Sr isotopes provide a solid interpretative basis for provenance and traceability studies. Our
373 maps and database are freely accessible online and will be updated in the future when new data become available.
374 In this sense, we will continue to collect and analyse new environmental samples from low-density areas (such as
375 Sicily and Sardinia) to improve the prediction power of the models. In addition, we plan to employ novel methods
376 for the spatial modelling of isotope data, using different predictors and machine learning approaches.

377

378 Acknowledgments

379 The Geochemistry Lab at the University of Modena and Reggio Emilia has been funded through a grant of the
380 Programma Giovani Ricercatori Rita Levi Montalcini to AC. This project received funds by the European
381 Research Council (ERC) under the European Union's Horizon 2020 Research and Innovation Programme
382 (grant agreement No 724046 – SUCCESS awarded to SB) and the MIUR FARE programme 2018 (FARE
383 Ricerca in Italia: Framework per l'attrazione e il rafforzamento delle eccellenze - SAPIENS project to SB). Mattia
384 Sisti is thanked for initiating the collection of Sr isotope data and Silvia Cercatillo for water sampling.

385

386 References

387 Adams, S., Grün, R., McGahan, D., Zhao, J., Feng, Y., Nguyen, A., Willmes, M., Quaresimin, M., Lobsey, B.,
388 Collard, M., 2019. A strontium isoscape of north-east Australia for human provenance and repatriation.
389 *Geoarchaeology* 34, 231–251.

390 Argentino, C., Lugli, F., Cipriani, A., Panieri, G., 2021. Testing miniaturized extraction chromatography
391 protocols for combined $^{87}\text{Sr}/^{86}\text{Sr}$ and $\delta^{88}/^{86}\text{Sr}$ analyses of pore water by MC-ICP-MS. *Limnol. Oceanogr.*
392 *Methods* 19, 431–440.

393 Bataille, C.P., Bowen, G.J., 2012. Mapping $^{87}\text{Sr}/^{86}\text{Sr}$ variations in bedrock and water for large scale provenance
394 studies. *Chem. Geol.* 304, 39–52.

395 Bataille, C.P., Von Holstein, I.C.C., Laffoon, J.E., Willmes, M., Liu, X.-M., Davies, G.R., 2018. A bioavailable
396 strontium isoscape for Western Europe: A machine learning approach. *PLoS One* 13, e0197386.

397 Bataille, C.P., Jaouen, K., Milano, S., Trost, M., Steinbrenner, S., Crubézy, É., Colleter, R., 2021. Triple sulfur-
398 oxygen-strontium isotopes probabilistic geographic assignment of archaeological remains using a novel sulfur
399 isoscape of western Europe. *PLoS One* 16, e0250383.

400 Bentley, R.A., 2006. Strontium isotopes from the earth to the archaeological skeleton: A review. *J. Archaeol.*
401 *Method Theory* 13, 135–187.

402 Bowen, G.J., 2010. Isoscapes: spatial pattern in isotopic biogeochemistry. *Annu. Rev. Earth Planet. Sci.* 38, 161–
403 187.

- 404 Britton, K., Le Corre, M., Willmes, M., Moffat, I., Grün, R., Mannino, M.A., Woodward, S., Jaouen, K., 2020.
405 Sampling Plants and Malacofauna in $^{87}\text{Sr}/^{86}\text{Sr}$ Bioavailability Studies: implications for isoscape mapping and
406 reconstructing of past mobility patterns. *Front. Ecol. Evol.* 8, 579473.
- 407 Capo, R.C., Stewart, B.W., Chadwick, O.A., 1998. Strontium isotopes as tracers of ecosystem processes: theory
408 and methods. *Geoderma* 82, 197–225.
- 409 Cardarelli, A., Cavazzuti, C., Quondam, F., Salvadei, L., Salzani, L., 2015. Le necropoli delle Narde di Frattesina:
410 proposta per una lettura delle evidenze demografiche, rituali e sociali a partire dai dati archeologici e antropologici.
411 Le necropoli delle Narde di Frat. *Propos. per una Lett. delle evidenze Demogr. Ritual. e Soc. a partire dai dati*
412 *Archeol. e Antropol.* 437–445.
- 413 Cavazzuti, C., Cardarelli, A., Quondam, F., Salzani, L., Ferrante, M., Nisi, S., Millard, A.R., Skeates, R., 2019a.
414 Mobile elites at Frattesina: flows of people in a Late Bronze Age ‘port of trade’ in northern Italy. *Antiquity* 93,
415 624–644.
- 416 Cavazzuti, C., Skeates, R., Millard, A.R., Nowell, G., Peterkin, J., Brea, M.B., Cardarelli, A., Salzani, L., 2019b.
417 Flows of people in villages and large centres in Bronze Age Italy through strontium and oxygen isotopes. *PLoS*
418 *One* 14, e0209693.
- 419 Cavazzuti, C., Hajdu, T., Lugli, F., Sperduti, A., Vicze, M., Horváth, A., Major, I., Molnár, M., Palcsu, L., Kiss,
420 V., 2021. Human mobility in a Bronze Age Vátya ‘urnfield’ and the life history of a high-status woman. *PLoS One*
421 16, e0254360.
- 422 Chesson, L.A., Tipple, B.J., Ehleringer, J.R., Park, T., Bartelink, E.J., 2018. Forensic applications of isotope
423 landscapes (“isoscapes”): a tool for predicting region-of-origin in forensic anthropology cases. *Forensic Anthropol.*
424 *Theor. Framew. Sci. basis* 127–148.
- 425 Colleter, R., Bataille, C.P., Dabernat, H., Pichot, D., Hamon, P., Duchesne, S., Labaune-Jean, F., Jean, S., Le
426 Cloirec, G., Milano, S., 2021. The last battle of Anne of Brittany: solving mass grave through an interdisciplinary
427 approach (paleopathology, biological anthropology, history, multiple isotopes and radiocarbon dating). *PLoS*
428 *One* 16, e0248086.

- 429 Copeland, S.R., Cawthra, H.C., Fisher, E.C., Lee-Thorp, J.A., Cowling, R.M., le Roux, P.J., Hodgkins, J.,
430 Marean, C.W., 2016. Strontium isotope investigation of ungulate movement patterns on the Pleistocene Paleo-
431 Agulhas Plain of the Greater Cape Floristic Region, South Africa. *Quat. Sci. Rev.* 141, 65–84.
- 432 Ehrlich, S., Gavrieli, I., Dor, L.-B., Halicz, L., 2001. Direct high-precision measurements of the $^{87}\text{Sr}/^{86}\text{Sr}$ isotope
433 ratio in natural water, carbonates and related materials by multiple collector inductively coupled plasma mass
434 spectrometry (MC-ICP-MS). *J. Anal. At. Spectrom.* 16, 1389–1392.
- 435 Emery, M. V, Stark, R.J., Murchie, T.J., Elford, S., Schwarcz, H.P., Prowse, T.L., 2018. Mapping the origins of
436 Imperial Roman workers (1st–4th century CE) at Vagnari, Southern Italy, using $^{87}\text{Sr}/^{86}\text{Sr}$ and $\delta^{18}\text{O}$ variability.
437 *Am. J. Phys. Anthropol.* 166, 837–850.
- 438 Erel, Y., Torrent, J., 2010. Contribution of Saharan dust to Mediterranean soils assessed by sequential extraction
439 and Pb and Sr isotopes. *Chem. Geol.* 275, 19–25.
- 440 Ericson, J., 1985. Strontium isotope characterization in the study of prehistoric human ecology. *J. Hum. Evol.* 14,
441 503–514.
- 442 Evans, J.A., Montgomery, J., Wildman, G., Boulton, N., 2010. Spatial variations in biosphere $^{87}\text{Sr}/^{86}\text{Sr}$ in
443 Britain. *J. Geol. Soc. London.* 167, 1–4.
- 444 Faure, G., Mensing, T.M., 2005. *Isotopes: principles and applications*, 3rd ed. John Wiley & Sons, Hoboken, New
445 Jersey.
- 446 Frank, A.B., Frei, R., Moutafi, I., Voutsaki, S., Orgeolet, R., Kristiansen, K., Frei, K.M., 2021. The geographic
447 distribution of bioavailable strontium isotopes in Greece—A base for provenance studies in archaeology. *Sci. Total*
448 *Environ.* 148156.
- 449 Frei, K.M., Frei, R., 2011. The geographic distribution of strontium isotopes in Danish surface waters - A base for
450 provenance studies in archaeology, hydrology and agriculture. *Appl. Geochemistry* 26, 326–340.
- 451 Funck, J., Bataille, C., Rasic, J., Wooller, M., 2021. A bio-available strontium isoscape for eastern Beringia: a tool
452 for tracking landscape use of Pleistocene megafauna. *J. Quat. Sci.* 36, 76–90.

- 453 Gregoricka, L.A., 2021. Moving Forward: A Bioarchaeology of Mobility and Migration. *J. Archaeol. Res.* doi:
454 10.1007/s10814-020-09155-9.
- 455 Han, G., Song, Z., Tang, Y., Wu, Q., Wang, Z., 2019. Ca and Sr isotope compositions of rainwater from Guiyang
456 city, Southwest China: Implication for the sources of atmospheric aerosols and their seasonal variations. *Atmos.*
457 *Environ.* 214, 116854.
- 458 Hartman, G., Richards, M., 2014. Mapping and defining sources of variability in bioavailable strontium isotope
459 ratios in the Eastern Mediterranean. *Geochim. Cosmochim. Acta* 126, 250–264.
- 460 Hedman, K.M., Slater, P.A., Fort, M.A., Emerson, T.E., Lambert, J.M., 2018. Expanding the strontium isoscape
461 for the American midcontinent: Identifying potential places of origin for Cahokian and Pre-Columbian migrants.
462 *J. Archaeol. Sci. Reports* 22, 202–213.
- 463 Hobson, K.A., Barnett-Johnson, R., Cerling, T., 2010. Using isoscapes to track animal migration, in: *Isoscapes*.
464 Springer, pp. 273–298.
- 465 Holt, E., Evans, J.A., Madgwick, R., 2021. Strontium ($^{87}\text{Sr}/^{86}\text{Sr}$) mapping: a critical review of methods and
466 approaches. *Earth-Science Rev.* 103593.
- 467 Hoogewerff, J.A., Reimann, C., Ueckermann, H., Frei, R., Frei, K.M., van Aswegen, T., Stirling, C., Reid, M.,
468 Clayton, A., Ladenberger, A., 2019. Bioavailable $^{87}\text{Sr}/^{86}\text{Sr}$ in European soils: A baseline for provenancing
469 studies. *Sci. Total Environ.* 672, 1033–1044.
- 470 Killick, D.J., Stephens, J.A., Fenn, T.R., 2020. Geological constraints on the use of lead isotopes for provenance
471 in archaeometallurgy. *Archaeometry* 62, 86–105.
- 472 Knudson, K.J., Williams, H.M., Buikstra, J.E., Tomczak, P.D., Gordon, G.W., Anbar, A.D., 2010. Introducing
473 $\delta^{88}\text{Sr}/^{86}\text{Sr}$ analysis in archaeology: a demonstration of the utility of strontium isotope fractionation in paleodietary
474 studies. *J. Archaeol. Sci.* 37, 2352–2364.
- 475 Kootker, L.M., van Lanen, R.J., Kars, H., Davies, G.R., 2016. Strontium isoscapes in The Netherlands. Spatial
476 variations in $^{87}\text{Sr}/^{86}\text{Sr}$ as a proxy for palaeomobility. *J. Archaeol. Sci. Reports* 6, 1–13.

- 477 Krige, D.G., 1951. A statistical approach to some basic mine valuation problems on the Witwatersrand. J. South.
478 African Inst. Min. Metall. 52, 119–139.
- 479 Ladegaard-Pedersen, P., Achilleos, M., Dörflinger, G., Frei, R., Kristiansen, K., Frei, K.M., 2020. A strontium
480 isotope baseline of Cyprus. Assessing the use of soil leachates, plants, groundwater and surface water as proxies
481 for the local range of bioavailable strontium isotope composition. Sci. Total Environ. 708, 134714.
- 482 Laffoon, J.E., Sonnemann, T.F., Shafie, T., Hofman, C.L., Brandes, U., Davies, G.R., 2017. Investigating human
483 geographic origins using dual-isotope ($^{87}\text{Sr}/^{86}\text{Sr}$, $\delta^{18}\text{O}$) assignment approaches. PLoS One 12, e0172562.
- 484 Lazzarini, N., Balter, V., Coulon, A., Tacail, T., Marchina, C., Lemoine, M., Bayarkhuu, N., Turbat, T., Lepetz,
485 S., Zazzo, A., 2021. Monthly mobility inferred from isoscapes and laser ablation strontium isotope ratios in
486 caprine tooth enamel. Sci. Rep. 11, 1–11.
- 487 Lightfoot, E., O’Connell, T.C., 2016. On the use of biomineral oxygen isotope data to identify human migrants
488 in the archaeological record: intra-sample variation, statistical methods and geographical considerations. PLoS
489 One 11, e0153850.
- 490 Lugli, F., Cipriani, A., Peretto, C., Mazzucchelli, M., Brunelli, D., 2017. In situ high spatial resolution $^{87}\text{Sr}/^{86}\text{Sr}$
491 ratio determination of two Middle Pleistocene (c.a. 580 ka) *Stephanorhinus hundsheimensis* teeth by LA–MC–
492 ICP–MS. Int. J. Mass Spectrom. 412, 38–48.
- 493 Lugli, F., Cipriani, A., Capecchi, G., Ricci, S., Boschini, F., Boscato, P., Iacumin, P., Badino, F., Mannino, M.A.,
494 Talamo, S., Richards, M.P., Benazzi, S., Ronchitelli, A., 2019. Strontium and stable isotope evidence of human
495 mobility strategies across the Last Glacial Maximum in southern Italy. Nat. Ecol. Evol. 3, 905–911.
- 496 Maurer, A., Galer, S.J.G., Knipper, C., Beierlein, L., Nunn, E. V, Peters, D., Tütken, T., Alt, K.W., Schöne, B.R.,
497 2012. Bioavailable $^{87}\text{Sr}/^{86}\text{Sr}$ in different environmental samples — Effects of anthropogenic contamination and
498 implications for isoscapes in past migration studies. Sci. Total Environ. 433, 216–229.
- 499 McArthur, J.M., Howarth, R.J., Bailey, T.R., 2001. Strontium isotope stratigraphy: LOWESS version 3: best fit
500 to the marine Sr-isotope curve for 0-509 Ma and accompanying look-up table for deriving numerical age. J. Geol.
501 109, 155–170.

- 502 Montgomery, J., Evans, J. a., Wildman, G., 2006. $^{87}\text{Sr}/^{86}\text{Sr}$ isotope composition of bottled British mineral waters
503 for environmental and forensic purposes. *Appl. Geochemistry* 21, 1626–1634.
- 504 Muhlfield, C.C., Thorrold, S.R., McMahon, T.E., Marotz, B., 2012. Estimating westslope cutthroat trout
505 (*Oncorhynchus clarkii lewisi*) movements in a river network using strontium isoscapes. *Can. J. Fish. Aquat. Sci.*
506 69, 906–915.
- 507 Négrel, P., Guerrot, C., Millot, R., 2007. Chemical and strontium isotope characterization of rainwater in France:
508 influence of sources and hydrogeochemical implications. *Isotopes Environ. Health Stud.* 43, 179–196.
- 509 Oliver, M.A., Webster, R., 1990. Kriging: a method of interpolation for geographical information systems. *Int. J.*
510 *Geogr. Inf. Syst.* 4, 313–332.
- 511 Pederzani, S., Britton, K., 2019. Oxygen isotopes in bioarchaeology: Principles and applications, challenges and
512 opportunities. *Earth-Science Rev.* 188, 77–107.
- 513 Pellegrini, M., Pouncett, J., Jay, M., Pearson, M.P., Richards, M.P., 2016. Tooth enamel oxygen “isoscapes” show
514 a high degree of human mobility in prehistoric Britain. *Sci. Rep.* 6, 34986.
- 515 Pestle, W.J., Simonetti, A., Curet, L.A., 2013. $^{87}\text{Sr}/^{86}\text{Sr}$ variability in Puerto Rico: geological complexity and the
516 study of paleomobility. *J. Archaeol. Sci.* 40, 2561–2569.
- 517 Pors Nielsen, S., 2004. The biological role of strontium. *Bone* 35, 583–8.
- 518 Scaffidi, B.K., Knudson, K.J., 2020. An archaeological strontium isoscape for the prehistoric Andes:
519 Understanding population mobility through a geostatistical meta-analysis of archaeological $^{87}\text{Sr}/^{86}\text{Sr}$ values
520 from humans, animals, and artifacts. *J. Archaeol. Sci.* 117, 105121.
- 521 Sillen, A., Hall, G., Richardson, S., Armstrong, R., 1998. $^{87}\text{Sr}/^{86}\text{Sr}$ ratios in modern and fossil food-webs of the
522 Sterkfontein Valley: implications for early hominid habitat preference. *Geochim. Cosmochim. Acta* 62, 2463–
523 2473.
- 524 Slovak, N.M., Paytan, A., 2012. Applications of Sr Isotopes in Archaeology, in: Baskaran, M. (Ed.), *Handbook of*
525 *Environmental Isotope Geochemistry*. Springer, pp. 743–768.

- 526 Smith, K.E., Weis, D., Amini, M., Shiel, A.E., Lai, V.W.-M., Gordon, K., 2019. Honey as a biomonitor for a
527 changing world. *Nat. Sustain.* 2, 223–232.
- 528 Snoeck, C., Ryan, S., Pouncett, J., Pellegrini, M., Claeys, P., Wainwright, A.N., Mattielli, N., Lee-Thorp, J.A.,
529 Schulting, R.J., 2020. Towards a biologically available strontium isotope baseline for Ireland. *Sci. Total Environ.*
530 712, 136248.
- 531 Song, B.-Y., Ryu, J.-S., Shin, H.S., Lee, K.-S., 2014. Determination of the source of bioavailable Sr using $^{87}\text{Sr}/^{86}\text{Sr}$
532 tracers: a case study of hot pepper and rice. *J. Agric. Food Chem.* 62, 9232–9238.
- 533 Soto, D.X., Wassenaar, L.I., Hobson, K.A., 2013. Stable hydrogen and oxygen isotopes in aquatic food webs are
534 tracers of diet and provenance. *Funct. Ecol.* 27, 535–543.
- 535 Thomsen, E., Andreasen, R., 2019. Agricultural lime disturbs natural strontium isotope variations: Implications
536 for provenance and migration studies. *Sci. Adv.* 5, eaav8083.
- 537 Tommasini, S., Marchionni, S., Tescione, I., Casalini, M., Braschi, E., Avanzinelli, R., Conticelli, S., 2018.
538 Strontium isotopes in biological material: A key tool for the geographic traceability of foods and humans beings,
539 in: *Behaviour of Strontium in Plants and the Environment*. Springer, pp. 145–166.
- 540 Toncala, A., Trautmann, B., Velte, M., Kropf, E., McGlynn, G., 2020. On the premises of mixing models to define
541 local bioavailable $^{87}\text{Sr} / ^{86}\text{Sr}$ ranges in archaeological contexts. *Sci. Total Environ.* 745, 140902.
- 542 Vautour, G., Poirier, A., Widory, D., 2015. Tracking mobility using human hair: What can we learn from lead
543 and strontium isotopes? *Sci. Justice* 55, 63–71.
- 544 Voerkelius, S., Lorenz, G.D., Rummel, S., Quézel, C.R., Heiss, G., Baxter, M., Brach-Papa, C., Deters-Itzelsberger,
545 P., Hoelzl, S., Hoogewerff, J., Ponzevera, E., Van Bocxstaele, M., Ueckermann, H., 2010. Strontium isotopic
546 signatures of natural mineral waters, the reference to a simple geological map and its potential for authentication
547 of food. *Food Chem.* 118, 933–940.
- 548 Wang, X., Tang, Z., 2020. The first large-scale bioavailable Sr isotope map of China and its implication for
549 provenance studies. *Earth-Science Rev.* 103353.

- 550 Washburn, E., Nesbitt, J., Ibarra, B., Fehren-Schmitz, L., Oelze, V.M., 2021. A strontium isoscape for the
551 Conchucos region of highland Peru and its application to Andean archaeology. *PLoS One* 16, e0248209.
- 552 Weber, M., Tacail, T., Lugli, F., Clauss, M., Weber, K., Leichliter, J., Winkler, D.E., Mertz-Kraus, R., Tütken, T.,
553 2020. Strontium uptake and intra-population $^{87}\text{Sr}/^{86}\text{Sr}$ variability of bones and teeth—controlled feeding
554 experiments with rodents (*Rattus norvegicus*, *Cavia porcellus*). *Front. Ecol. Evol.* 8, 569940.
- 555 Willmes, M., Bataille, C.P., James, H.F., Moffat, I., McMorrow, L., Kinsley, L., Armstrong, R.A., Eggins, S.,
556 Grün, R., 2018. Mapping of bioavailable strontium isotope ratios in France for archaeological provenance studies.
557 *Appl. Geochemistry* 90, 75–86.
- 558 Yanes, Y., Delgado, A., Castillo, C., Alonso, M.R., Ibáñez, M., De la Nuez, J., Kowalewski, M., 2008. Stable
559 isotope ($\delta^{18}\text{O}$, $\delta^{13}\text{C}$, and δD) signatures of recent terrestrial communities from a low-latitude, oceanic setting:
560 endemic land snails, plants, rain, and carbonate sediments from the eastern Canary Islands. *Chem. Geol.* 249,
561 377–392.
- 562 Zieliński, M., Dopieralska, J., Królikowska-Ciągło, S., Walczak, A., Belka, Z., 2021. Mapping of spatial variations
563 in Sr isotope signatures ($^{87}\text{Sr}/^{86}\text{Sr}$) in Poland—Implications of anthropogenic Sr contamination for
564 archaeological provenance and migration research. *Sci. Total Environ.* 775, 145792.
- 565

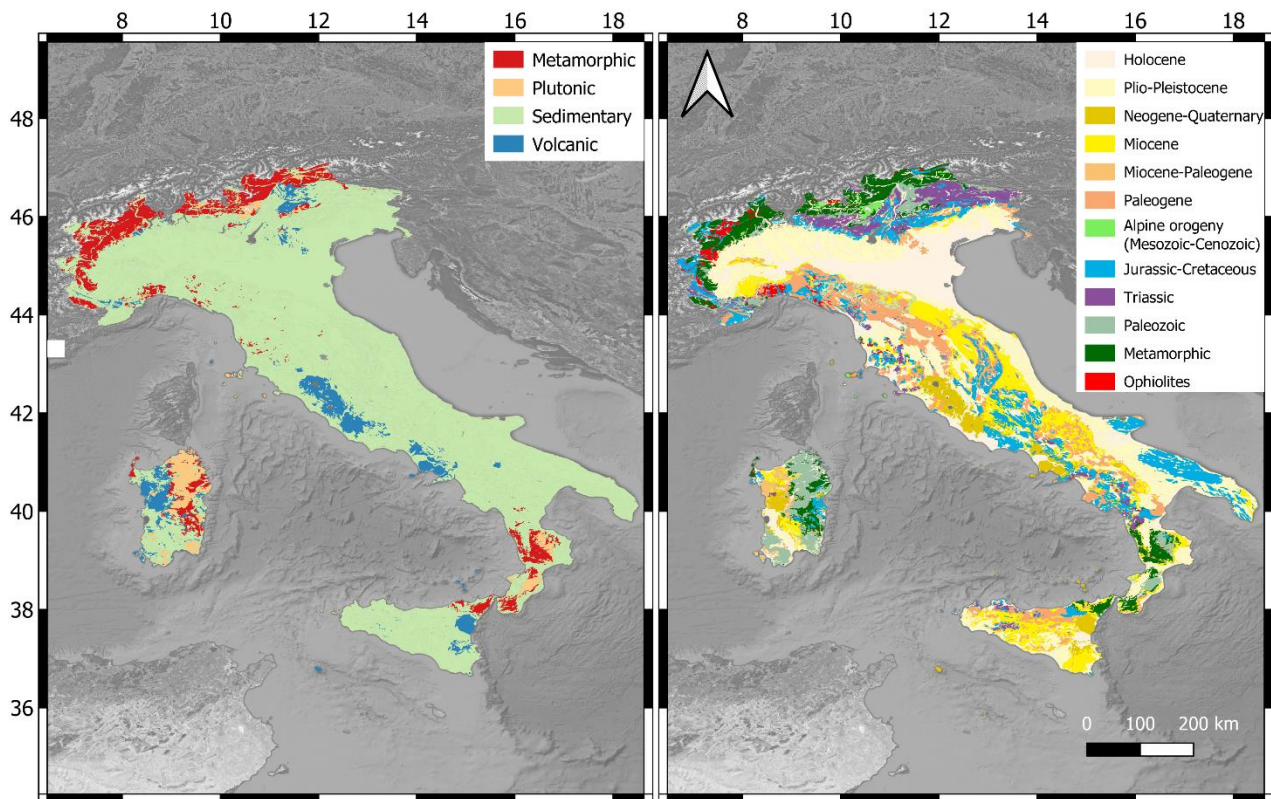


Figure S1. Geological maps of Italy. Left panel: formations are categorized by rock 'family'. Right panel: formations are categorized by age. This map is based on the geolithological map of Italy available at the Geoportale Nazionale (http://wms.pcn.minambiente.it/ogc?map=/ms_ogc/wfs/Carta_geolitologica.map); the satellite map is provided by Google through the QGIS QuickMapServices plug-in.

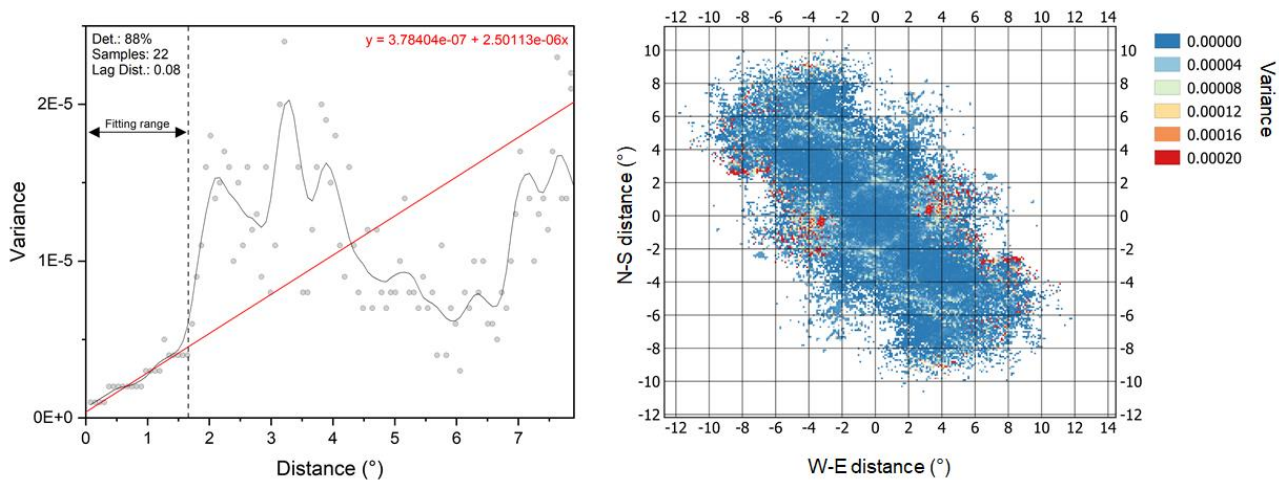


Figure S2. 'Bioavailable' Ordinary Kriging variogram (biplot and surface) obtained through SAGA 7.9.

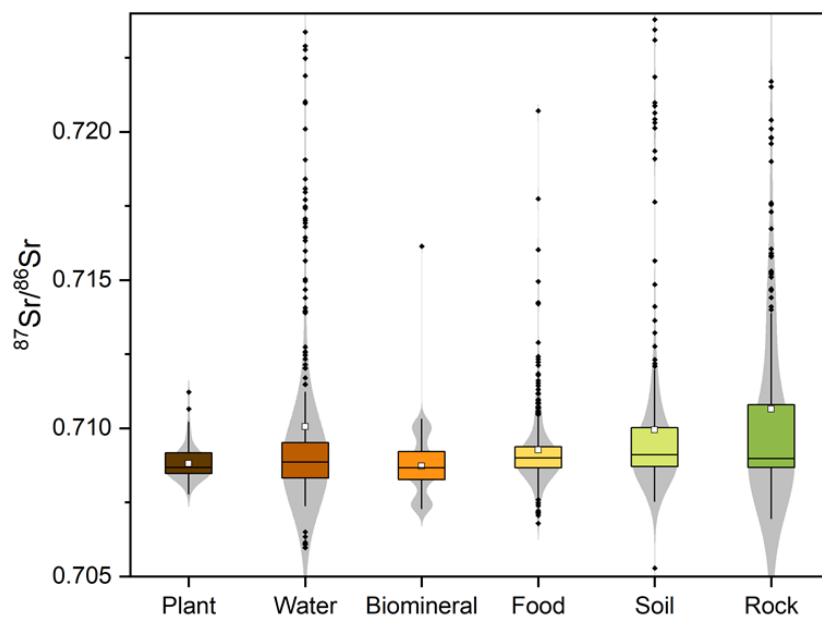


Figure S3. Box plot graph representing the $^{87}\text{Sr}/^{86}\text{Sr}$ ratios of the different sample categories. The gray shadows are data distributions obtained by kernel density estimations. Note that the graph is cut at 0.724 to improve readability, with some outliers plotting beyond the graph range.

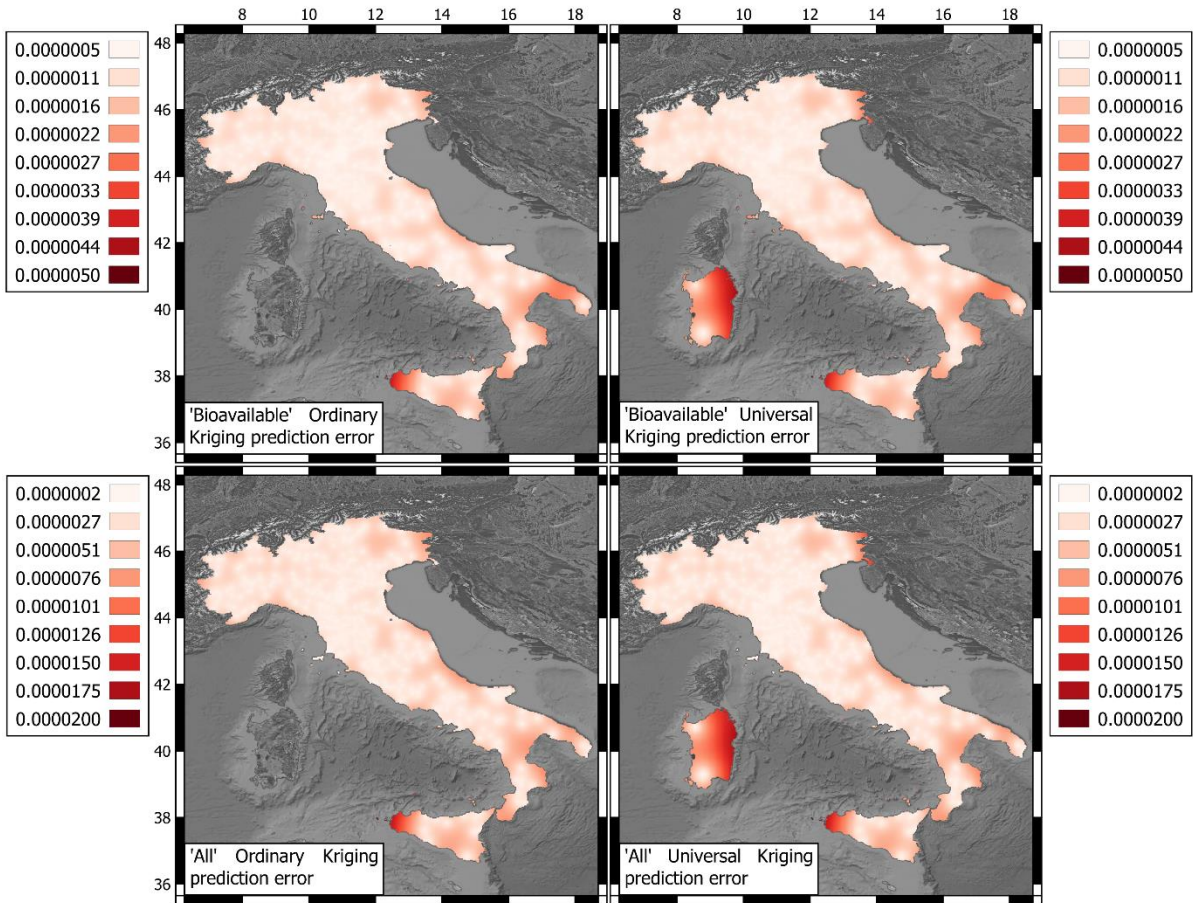


Figure S4. Prediction standard error for the Kriging models. Maps were obtained using SAGA 7.9 and QGIS 3.8.

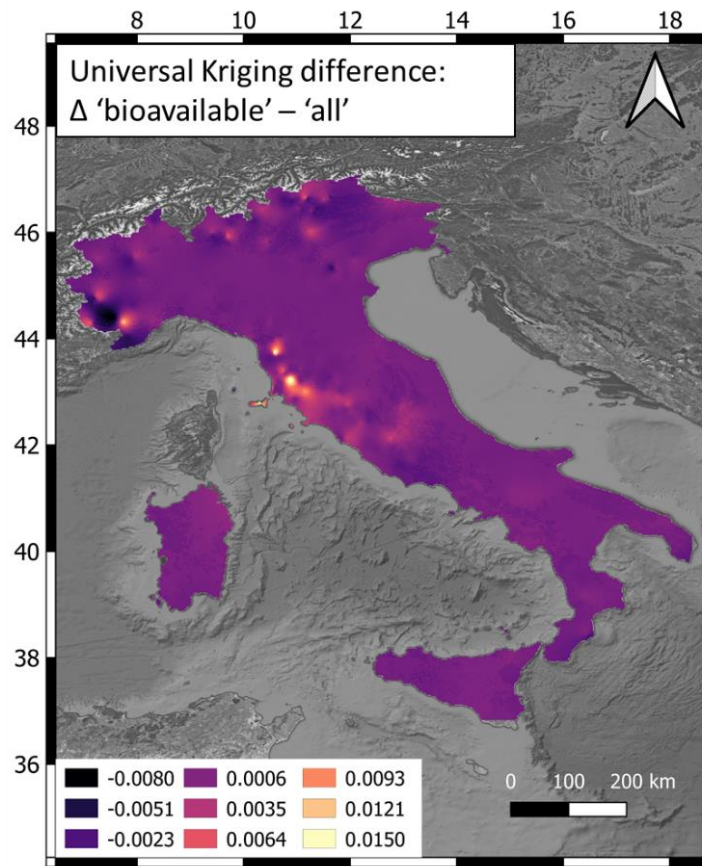


Figure S5. $^{87}\text{Sr}/^{86}\text{Sr}$ difference between 'all' and 'bioavailable' Universal Kriging models; e.g. a positive value means that Sr isotope data are higher in the 'all' map. Maps were obtained using SAGA 7.9 and QGIS 3.8.

Table S1. Descriptive statistics for the whole dataset and (non-)bioavailable samples. 'Bioavailable' samples are 'plant', 'water', 'biomineral' and 'food' categories, in addition to 'soil' leachates. 'Non-bioavailable' samples are 'rock' and bulk 'soil'.

Category	N total	Mean	2 SD	Minimum	Median	Maximum	Interquartile Range (Q3 - Q1)
'Bioavailable'	1568	0.70941	0.00632	0.70354	0.70883	0.76384	0.00091
'Non-bioavailable'	352	0.71069	0.01054	0.70319	0.709	0.753	0.00223
'All'	1920	0.70964	0.00734	0.70319	0.70888	0.76384	0.00105